MATERIALS SCIENCE

Atoms to fibers: Identifying novel processing methods in the synthesis of pitch-based carbon fibers

Asmita Jana[1], Taishan Zhu[1], Yanming Wang[1], Jeramie J. Adams[2], Logan T. Kearney[3], Amit K. Naskar[3], Jeffrey C. Grossman[1], Nicola Ferralis[1]*

Understanding and optimizing the key mechanisms used in the synthesis of pitch-based carbon fibers (CFs) are challenging, because unlike polyacrylonitrile-based CFs, the feedstock for pitch-based CFs is chemically heterogeneous, resulting in complex fabrication leading to inconsistency in the final properties. In this work, we use molecular dynamics simulations to explore the processing and chemical phase space through a framework of CF models to identify their effects on elastic performance. The results are in excellent agreement with experiments. We find that density, followed by alignment, and functionality of the molecular constituents dictate the CF mechanical properties more strongly than their size and shape. Last, we propose a previously unexplored fabrication route for high-modulus CFs. Unlike graphitization, this results in increased sp^3 fraction, achieved via generating high-density CFs. In addition, the high sp^3 fraction leads to the fabrication of CFs with isometric compressive and tensile moduli, enabling their potential applications for compressive loading.

INTRODUCTION

Carbon fibers (CFs) are beneficial in a range of industries such as aerospace, automobile, and sports equipment, because of their low weight but high modulus, strength, and chemical resilience (*1*–*3*). Yet, because of high cost compared with alternative materials such as glass and plastic fibers, the widespread deployment of CFs has been limited to niche applications, such as in aerospace applications that use the CFs' superior mechanical properties and heat resistance (*1*, *4*). The cost of CFs is 4 to 6 times that of aluminum and 15 to 20 times that of steel (*5*–*7*). A substantial reduction in cost may be possible by adopting cheaper initial feedstocks and low-temperature processing methods. Now, more than 96% of CFs use polyacrylonitrile (PAN) as precursor, which is made from polymeric fibers of a petrochemical product called acrylonitrile, while the remaining use pitch, which is a viscoelastic material derived from fossil fuels (*4*, *5*, *8*). The lower cost of pitch [coal tar pitch (CTP), \$800/ton (*9*); petroleum pitch (PP), \$400/ton (*10*)] compared with PAN (\$2100/ton to \$2250/ton) (*11*) as a precursor material (*1*, *4*) may ultimately provide a viable route for manufacturing CFs at \$11/kg (*5*). In addition, conventional PAN precursor fiber processing requires a series of unit operations involving organic solution of PAN polymer and subsequent solvent recovery (*12*). In contrast, pitch feedstocks can be melt processed to make fibers, and such precursor processing routes require less capital investment (*13*). However, the heterogeneous nature of pitch and the variability in which such heterogeneity is expressed among the used pitch feedstocks (*14*) often lead to inconsistent mechanical performance, requiring ad hoc, customized fabrication parameters highly dependent on the pitch itself. A major factor contributing to the difficulty and cost of the procedure is the often required conversion of pitch from isotropic to mesophase, because CFs derived from isotropic pitch usually have poorer mechanical properties (*14*). Isotropic pitch refers to a state where the molecular constituents are randomly oriented in the bulk, while mesophase pitch consists of molecules aligned in a preferred orientation, which leads those to behave like liquid crystals in molten state (*15*). In essence, reconciling the heterogeneous nature of the precursors and the intrinsic chemical variability in pitch feedstocks (Fig. 1) with a streamlined, generalized even if complex fabrication procedure with predictable performance (such as elastic modulus) requires the identification of how the properties of pitch during fabrication affect the final CF (*16*), leading to improved processing routes for low-cost, high-performance CFs.

The CF manufacturing process (*14*) from pitch usually involves four steps: melt spinning, stabilization, carbonization, and graphitization (*14*, *15*), and it is sensitive to the chemical nature of the pitch feedstock, temperature, processing time, and rates. First, pitch is melt spun to obtain continuous and drawable fibers with mesophase oriented along the fiber axis. Next, the drawn fibers undergo stabilization, which is an oxidization process at temperatures of around 200° to 300°C, to convert fibers from thermoplastic to thermoset, by facilitating aromatization and cross-linking in pitch molecules. During carbonization, the fibers are heated in an inert atmosphere to temperatures higher than 500°C, resulting in mass loss because of evolution of gases (H_2O and CO_2) accompanied with C-C bridges replacing some of the oxygen bridges between the mesophase molecules (*14*, *17*). During graphitization, the system is heated to temperatures around 2500° to 3000°C, facilitating the formation of larger graphitic crystalline structures, resulting in high modulus (> 300 GPa), thermal conductivity, electrical conductivity, tensile strength, etc. The high graphitization temperatures contribute to the overall cost of the procedure [graphitization alone costs \$0.70/kg for CTP CFs (*18*)]: Thus, a novel process leading to high-modulus CFs without resorting to graphitization may lead to a reduction in overall fabrication cost and associated energy and emissions requirements.

Given the large parametric space present in the manufacturing process and the need to predict properties based on the processing route, atomistic modeling can provide a route for decoupling the highly convoluted materials and processing parameter phase space. Molecular dynamics (MD) has been used to model the carbonization

[1]Department of Materials Science and Engineering, Massachusetts Institute of Technology, Cambridge, MA, USA. [2]Western Research Institute, Laramie, WY, USA. [3]Carbon and Composites Group, Chemical Sciences Division, Oak Ridge National Laboratory, Oak Ridge, TN, USA.
*Corresponding author. Email: ferralis@mit.edu

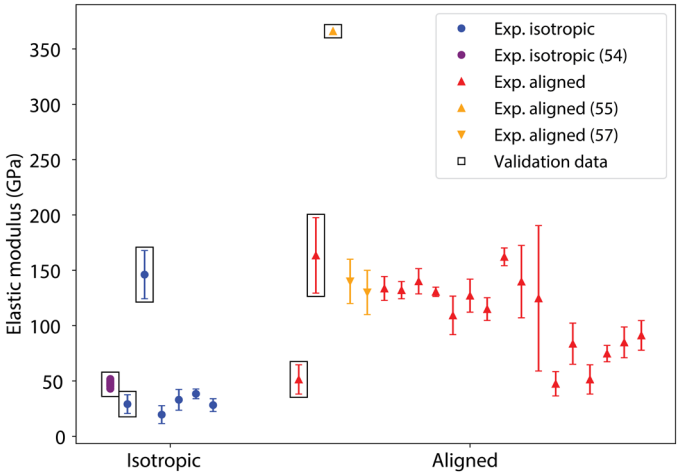

Fig. 1. Variability in range of elastic moduli. The variability in the range of elastic moduli observed for CFs made from CTP can be difficult to assess experimentally in relation to chemistry/processing and limits development of consistent manufacturing methods. Furthermore, identifying the origin, whether in the chemical makeup of the pitch or in the fabrication conditions (including outliers such as high modulus isotropic CF), requires a deconvolution of the interrelated roles played by the chemistry and structure of the pitch during CF fabrication. Selected data points (encapsulated by a rectangle) have been used for validation of the predictive models developed in this work.

process (*19*–*21*) and, specifically, the microstructure (*22*) in PAN-based CFs. In most of the recent modeling work, an idealized ladder structure was used to model the molecules (*22*–*24*), where the system was compressed to induce self-organization and generate CFs. Unlike the PAN-based CFs, the heterogeneity of the precursor pitch molecules because of its structure and chemical functionality makes it difficult to model pitch-based CFs, and most prior modeling work has made some assumptions regarding the initial molecular composition. Senda *et al.* (*25*) considered four initial pitch molecules: pyrene, triphenylene, fluorene, and 9-methylanthracene, while Jian *et al.* (*26*) used several naphthalene-based systems. Such simplification of geometry, structure, and chemical composition in the CF precursors (*22*–*26*) can limit both the breadth of materials space and the predictive accuracy as well as the ability to compare one set of results to another.

In this work, we take a different approach, by using an experimentally derived and validated parametric modeling framework with predictive capabilities for the manufacturing of pitch-based CFs. Our framework uses MD simulations with ReaxFF to describe interatomic forces, to generate and test for mechanical performance of an expansive range of CF models with varying degrees of stabilization, carbonization, and graphitization; the results are in excellent agreement with experiments. Unlike the classical force field, the ReaxFF can model empirical, bond-order–dependent reactions of complex materials by casting the potential in a bond-order formalism. Its computational costs are almost as low as the simple force fields while retaining the accuracy of quantum mechanics (*27*). While ReaxFF was developed mainly for combustive processes (*27*), we have adapted it to modeling stabilization by using a rule-based strategic procedure instead, which simulates the type of reactions observed in the stabilization and carbonization process and minimizes the reliance on model-specific reactions. There are three major characteristics of this approach that make it unique. First, this framework is aimed at exploring the experimental parametric phase space through the use of experimentally derived input parameters for materials structure and chemistry and fabrication processes: For example, the heterogeneity in pitch precursor structure and chemical functionality is realistically evaluated by identifying proxy compounds for both PP and CTP samples from experimental data. Second, with the help of this setup, we can also determine which parameters play a more important role in determining tensile modulus. For the selected molecular sets, we find that density, alignment, and functionality of the molecular constituents all play an essential role in the CF mechanical properties, while the size and shape play a less important role within the limits imposed by the MD method and the initial specific choice for the molecular set. Last, the robustness of the framework makes it possible to explore large regions of phase space, which might be otherwise unexplored, and to hypothesize novel synthesis strategies that can potentially lead to high-modulus CFs. For example, we observed that increasing the density of the CFs beyond the expected value for graphitic materials and into sp^3 carbon materials results in higher modulus (~400 GPa), suggesting an alternative path for high-modulus fibers other than graphitization. Furthermore, our simulations show that high sp^3 fraction in the ultrahigh-density CFs produced via the new route resulted in PP-based CFs with isometric compressive and tensile moduli, which could enable applications for CFs that rely on compressive modulus.

RESULTS

Both CTP and PP were separately studied in this work. While both CTP and PP are composed of predominantly fused aromatic molecules, PP contains additional methyl groups decorating the aromatic cores (*28*). The intrinsic molecular heterogeneity of pitch, however, required a careful selection of proxy molecular compounds for both PP and CTP that were validated experimentally. This was achieved in this study by selecting molecular constituents directly from mass spectroscopy (section S10) (*29*–*33*). While it was expected that differences in the typology and concentration of constituents would affect the fabrication of CFs and their performance, we found that the actual molecular distribution varied negligibly across different samples within either PP or CTP (section S10). To test the effects of molecular choice, including how different portions of the distribution of molecules may affect the outcome, we designed two sets of initial molecules for CTP. The first CTP set consisted of a polydisperse distribution of small molecules in the molecular weight range of 150 to 300 g/mol, referred henceforth as small polydisperse precursor molecules of CTP (small p-CTP) (Fig. 2A). The second CTP set consisted of a polydisperse distribution of relatively larger molecules in the molecular weight range of 200 to 450 g/mol, with 75% molecules in the molecular weight range of 300 to 450 g/mol, referred to as large polydisperse precursor molecules of CTP (large p-CTP) (Fig. 2A). While constituents with molecular weight lower than 200 g/mol get distilled out, we included some molecules in the 150 to 200 g/mol in the small p-CTP to study the impact of size of precursors on the properties. When considering PP, which also contains methyl functional groups (*28*), in addition to the aromatic cores, we wanted to study the effect of methyl groups on mechanical properties. To aid CF formation, molecular ensembles for PP from experimental mass spectrometry (section S10) were used to design

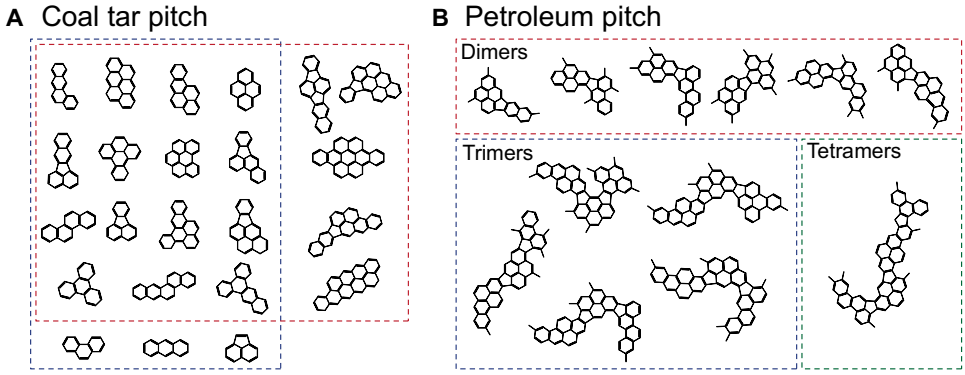

Fig. 2. Pitch precursor molecules. Selected set of experimentally inspired molecular compounds used as the initial set representing pitch. (**A**) CTP: Simplified molecular ensemble for p-CTP, grouped in subsets for smaller (enclosed by blue dashed region) and larger molecules (enclosed by red dashed region). (**B**) PP: The PP ensemble is composed of dimers, trimers, and tetramers.

a PP set composed of molecules highlighted in Fig. 2B. We chose molecules from PP mesophase instead of PP because we wanted to ensure that the number of methyl groups present was not too numerous to hinder the simulation of cross-linking reactions. As pointed out by Jian *et al.* (*26*, *34*), the presence of monomers with methyl groups translated to a larger fraction of methyl groups for a given aromatic core, which was relatively stable at carbonization conditions and could hinder the formation of larger structures. Here, we considered a polydisperse distribution of 30, 40, and 30 weight % of dimers, trimers, and tetramers, respectively, referred to as polydisperse precursor molecules of PP (p-PP). While including a higher concentration of larger molecules can result in a better representative sample for PP, we chose to model up to tetramers, because modeling systems with larger molecules than that would be more computationally intensive. Moreover, we found that smaller molecules were able to capture the trends in elastic modulus and displayed excellent agreement with experimental data.

One of the objectives of our study was to determine and therefore prioritize the impact that different initial proxy sets of molecules and their features (such as shape, size, and distribution) have on the final elastic modulus. This required the exploration of the feature phase space, through the design of 10 additional CTP systems composed of monodisperse distributions of each molecule depicted in fig. S1 (section S0). These additional systems were either composed of increasing sizes of elongated or circular molecules, henceforth referred to as elongated monodisperse precursor molecules of CTP (elongated m-CTP) and circular monodisperse precursor molecules of CTP (circular m-CTP), respectively. Another objective of this work was to investigate the role of the initial molecular alignment on the bonding configuration in the final CFs and their elastic properties. We accomplished this by creating two different systems for each of the 13 initial molecular sets, one where the molecules were randomly packed, termed isotropic, and the other where the molecules were placed such that all of them are parallel to a fixed plane, termed aligned. This is depicted in Fig. 3. The initial alignment was set manually, and the same procedure was used for all the pitch precursor sets. The overall set is composed of 26 systems. To ensure that we captured the behavior for these amorphous systems to a good degree of accuracy, we used five different starting configurations for each of these 26 systems.

In this work, we used MD simulations with ReaxFF to generate CFs and subsequently calculated elastic modulus based on a

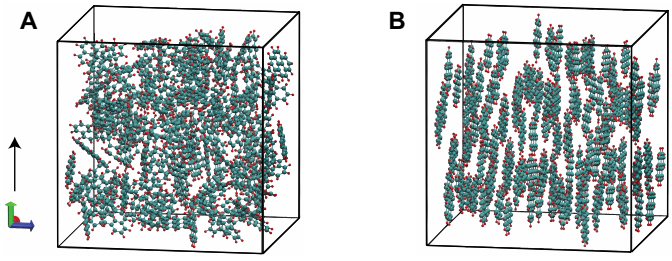

Fig. 3. Initial alignment of the precursor molecules. Precursor molecules are aligned (**A**) in a random orientation to simulate isotropic pitch and (**B**) parallel to the *xy* plane to simulate aligned pitch; black arrow indicates longitudinal direction.

stress-strain relationship (see section S1 for details). Our MD models were at the nanoscale level, and hence, these graphitic structures were a nanoscale representation of realistic CFs. We still referred to them as CFs because the tensile moduli computed out of this framework were representative for realistic CFs and were comparable to experimental values. A random packing was used for isotropic systems, whereas in aligned systems, the molecules were oriented along the *xy* plane, as highlighted in Fig. 3. As previously suggested (*14*, *17*, *35*), during stabilization, there is an uptake of oxygen (~6 to 7 atomic %) that leads to formation of carbonyls, hydroxyls, carboxylic acids, ethers, esters, and anhydrides, which later react and result in cross-linking during the carbonization process. The oxygen incorporated in the oxygen-containing functional groups formed during the stabilization step is removed in the carbonization step.

Because ReaxFF was developed mainly for combustive processes (*27*), using it directly to model stabilization can require additional validation of the products produced by the simulation using experiments (*25*). ReaxFF can capture an entire array of reactions, but without any overarching rule placed on it, it becomes very important to verify every reaction pathway, which can become very challenging. Senda *et al.* (*25*) recommended using techniques like infrared (IR) spectroscopy to gauge the accuracy of ReaxFF potentials when using it to model oxidation explicitly. In their work, they used IR spectroscopy to verify the oxidized products of each of the four precursor molecules separately and found that some of their computed results did not correlate with experiments, a difference attributed to sensitivity of the simulations to the environment. Jian *et al.*

(*26*) also emphasized experimental validation of the simulation products when investigating large-scale interconnectivity. In this work, we circumvented adding oxygen explicitly to avoid this challenge associated with modeling the stabilization step directly.

Instead, the direct cause-effect in bonding mediated by oxygen was captured in our simulations by facilitating the cross-linking of aromatic cores, without introducing any oxygen, when the distance and orientation between the aromatics were optimum for bonding. In this framework, which combined the stabilization and carbonization steps, sites at the edge of the aromatic molecules were activated by removing a fraction (default is 95%) of the hydrogen atoms at the start of the simulation. By using this rule-based method with ReaxFF, we were able to simulate the type of reactions observed in the stabilization and carbonization process and minimize the reliance on model-specific reactions. Moreover, the fraction of H atoms removed correlated with the number of sites available for cross-linking and can be correlated with the amount of oxygen used for the reactions; a higher oxygen uptake during stabilization can be simulated by increasing the fraction of H atoms removed. Thus, the fraction of H atoms removed acted as a proxy for the extent of stabilization and carbonization and became an effective tuning parameter to evaluate its effect on elastic modulus.

In addition to aromatic cores, PP is characterized by the decoration with the methyl functional groups (*28*), which often act as molecular bridges forming dimers, trimers, and tetramers (Fig. 2B). In the case of PP, as both aromatic and aliphatic H were present, the effects of H-removal on the stabilization and carbonization steps were more nuanced as the different chemical nature of aliphatic and aromatic H could affect the reactions taking place during those steps. Therefore, the selective removal of either type of H atom provided a template to study the effect of each type of H on the stabilization and carbonization reactions required in the synthesis of CF, as well as on the resulting elastic modulus of the CF. With no prior assumption on the preferred reactivity of each H site, four different reaction pathways were designed for PP. Pathway 1 corresponded to the case where 95% of both aliphatic and aromatic H atoms were removed. Pathways 2 and 3 represented the cases where 95% of only aliphatic H and only aromatic H were removed, respectively. In pathway 4, we first removed 95% of aliphatic H and subsequently removed 95% of aromatic H. During stabilization, it is hypothesized (*17*, *35*) that the aliphatic groups oxidize first, followed by aromatic cores, motivating the design of pathway 4. Because both aliphatic and aromatic groups take part in oxidation, we expected pathways 1 and 4 to be the more physically realistic compared with the other two pathways.

Coal tar pitch

In general, we observed that elastic modulus monotonically increased with density for all the systems. This relationship is depicted in Fig. 4 (A and B) for the CTP systems. The computed density was of the final system after the stabilization and carbonization steps (and graphitization, if applicable). We noted that experimental densities

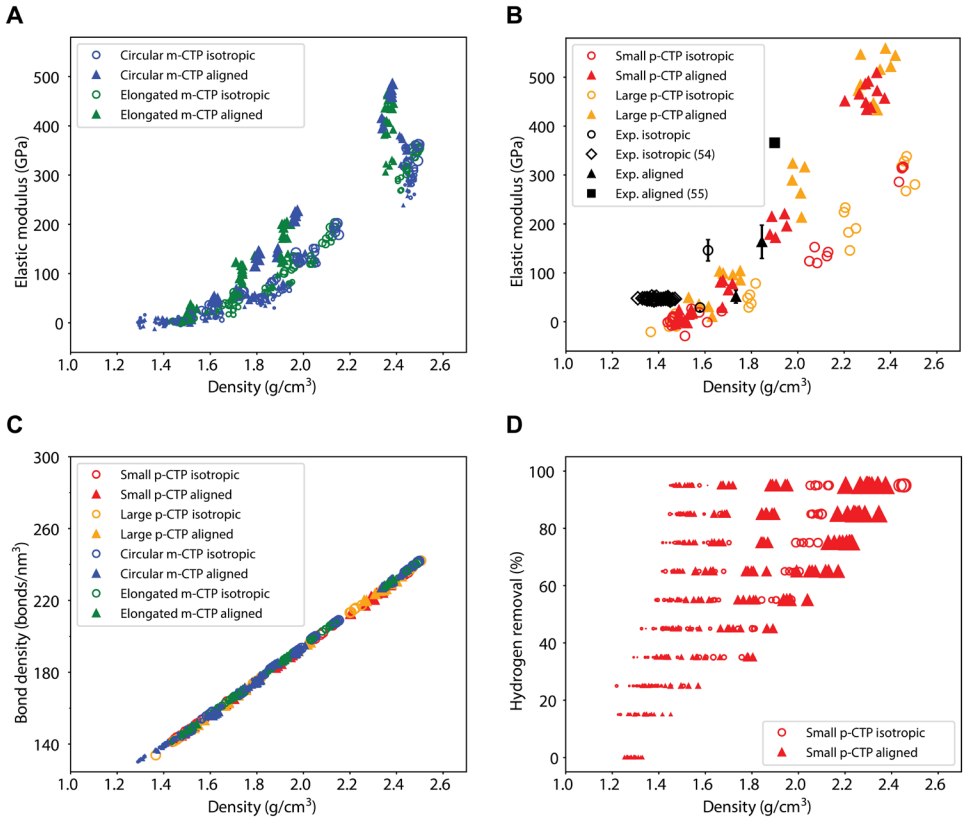

Fig. 4. CTP: Elastic modulus, density, bond density, and hydrogen removal. Elastic modulus versus density for the (**A**) m-CTP systems (the size of the points is proportional to the size of the initial molecules) and (**B**) p-CTP systems, (**C**) bond density versus density for all the CTP systems, and (**D**) elastic modulus as a function of hydrogen removal and density (the size of the points is proportional to the modulus) for the small p-CTP system.

were based on measurements that included larger-scale effects not captured within our nanoscale simulation cell, such as the presence of microvoids (~3% volume fraction) (*36*), which resulted in slightly higher computed densities compared with experiment. The number of bonds was another factor that affected the elastic modulus. However, we found that the bond density (number of bonds per unit volume) was constant at a given density for all CTP systems, regardless of size, shape, alignment, or dispersity of the initial molecules, as depicted in Fig. 4C. Another general trend observed was that aligned CFs displayed higher modulus when compared with isotropic CFs of the same initial molecular set. Because the bond density was unchanged, the computed difference in modulus was solely due to the difference in alignment. In addition to the elastic modulus, we also calculated the tensile transverse modulus, shear modulus, and Poisson's ratio (sections S6 and S8).

Next, to look more specifically into the effects of size and shape of initial molecules in isolation, we considered the monodisperse CTP system (Fig. 4A). First, we observed that the elastic modulus was independent of shape of the initial molecules, as both circular m-CTP and elongated m-CTP followed a similar trend. However, size differences of the initial molecules resulted in marked differences in modulus. In particular, for a given size and alignment, the larger the size of the initial molecules, the larger was the resultant modulus. The observation of size being a factor in determining modulus can be ascribed to the larger molecules retaining more alignment when compared with the smaller molecules. In addition, because at a given density the bond density was the same for all the molecular sets, regardless of shape, size, and alignment of the initial molecules (Fig. 4C), we were able to isolate the effects of size, shape, and alignment in the m-CTP sets.

While size played a role in determining modulus for m-CTP CFs, both small p-CTP and large p-CTP displayed similar trends in modulus, as depicted in Fig. 4B. In polydisperse systems, the sizes and shapes of the initial molecules did not play as large a role as other factors like density and alignment. Thus, in PP systems, we focused on functional groups instead of size, shape, and distribution of initial molecules. Moreover, we observed good agreement with the modulus for experimental CFs (section S9) at the same density. In some cases, our framework was able to predict moduli within 15% of the ones reported by experiments, although agreement with experiments was not as good at lower densities, which can be attributed to pyrolytic hydrocarbon mass loss other than hydrogen that has been considered in this study, resulting in higher porosity and higher error in experimental density measurements of relatively lower densities. When comparing modulus of m-CTP CFs with that of p-CTP CFs, we observed a relatively smaller modulus for the former. This can be attributed to higher packing efficiency of polydisperse distributions when compared with monodisperse distributions in general (*37*).

Furthermore, we varied the hydrogen removal fraction from 0 to 95% to simulate varying the oxygen uptake during stabilization. Higher fraction of hydrogen removal corresponded to more reactions, achieved via either aromatic condensation or oxygen-mediated cross-linking. The resulting elastic modulus as a function of hydrogen removal and density is plotted in Fig. 4D, with the size of the data points proportional to the modulus. Higher modulus was observed at higher hydrogen removal fractions, for both isotropic and aligned CFs. Because the hydrogen removal fraction can be correlated with the amount of oxygen uptake or the extent of stabilization, this was substantiated by the observation that understabilized CFs displayed lower modulus compared with their stabilized counterparts (*38*).

Petroleum pitch

Similar to CTP, the elastic modulus for p-PP also increased with increasing density, as depicted in Fig. 5A. In contrast to CTP, the bond density was not constant for a given density for all the p-PP sets, as shown in Fig. 5C. While the PP CFs generated from pathways 1 and 4 (both H removed) showed similar bond density, pathways 2 (only aliphatic H removed) and 3 (only aromatic H removed) led to slightly higher values because of additional unremoved C—H bonds. Despite higher bond density, pathways 2 and 3 led to lower modulus compared with pathways 1 and 4, as illustrated by Fig. 5A. Overall, the differences in modulus effectively arose from the number of active sites available or how many H atoms get removed. This emphasized the importance of both aromatic and aliphatic H in taking part in the reaction to form CFs, as not allowing both types of H to take part in the reaction can result in lowered modulus. A similar result has been observed by Zang *et al.* (*39*); both aliphatic groups and aromatic cores were shown to be important for cross-linking reactions and graphitic stacking.

Similar to CTP, we also varied the hydrogen removal fraction from 0 to 95% for the p-PP pathway 1 system. The resulting elastic modulus as a function of hydrogen removal and density is plotted in Fig. 5D, with the size of the points proportional to the modulus. Similar to CTP, we observed higher modulus at higher hydrogen removal fractions for both isotropic and aligned CFs.

Obtaining high-modulus CFs at ultrahigh density (beyond 2.2 g/cm^3) does not preclude the ability to obtain high-modulus CFs at lower densities consistent with graphitization. To verify this, we simulated an additional graphitization step on the aligned p-PP pathway 1 CFs with calculated modulus depicted in Fig. 5B. We found that simulating graphitization at a temperature of 3100 K provided the maximum modulus, and the data points corresponding to graphitized CFs in Fig. 5B correspond to graphitization at 3100 K, but at different graphitization times. The modulus increased with increasing graphitization time until it saturated at 100 ps (section S4). We found good agreement with experimental data (section S9) (*40*), as depicted in Fig. 5B, illustrating the ability of our computational framework to capture not only stabilization and carbonization but also graphitization.

We were able to discern two paths that can lead to high-modulus fibers, of which one is the well-established graphitization process. While graphitization (red solid line in Fig. 5B) requires a high-temperature heat treatment, the alternative procedure to producing high-modulus CFs, as illustrated by the blue solid line in Fig. 5B, involves producing CFs at higher densities.

Effects of density and hybridization on tensile and compressive moduli

While graphitization results in increased sp^2 bonds, the situation at higher densities is relatively unknown. To investigate the nature of bonding at these high densities, we calculated the change in fraction of sp^2 and sp^3 bonds in the CFs using Eqs. 1 and 2

$$\text{change in sp}^2\text{ fraction} = \frac{\text{final sp}^2\text{ fraction} - \text{initial sp}^2\text{ fraction}}{\text{initial sp}^2\text{ fraction}} \quad (1)$$

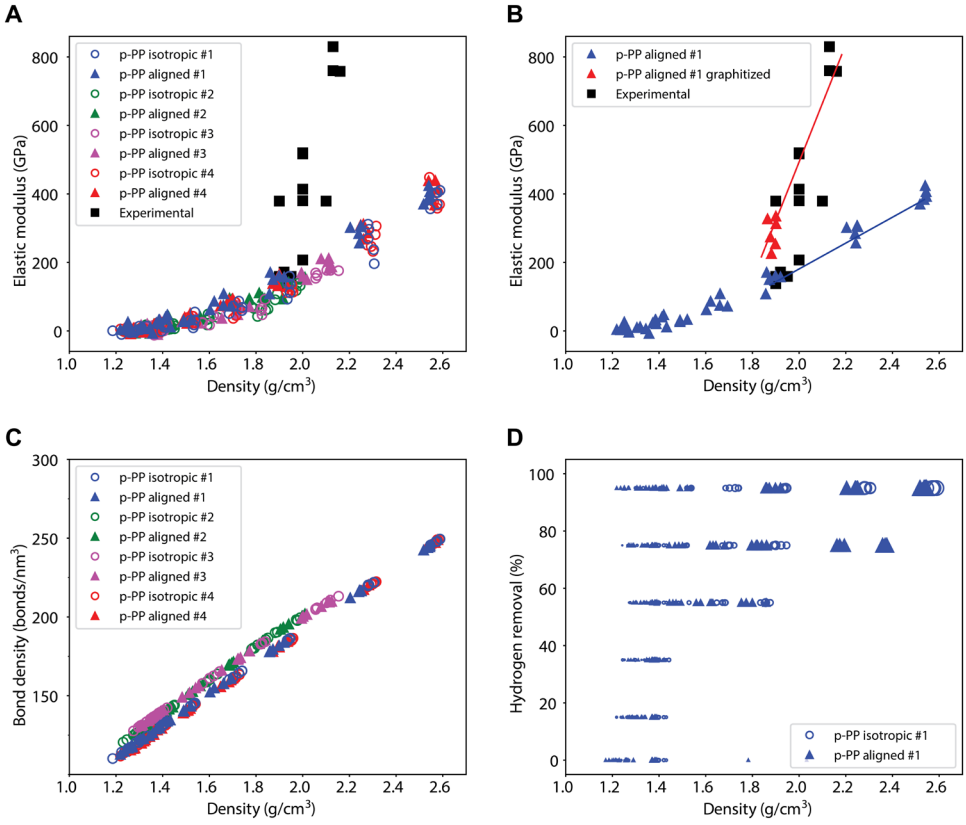

Fig. 5. PP: Elastic modulus, density, bond density, and hydrogen removal. Elastic modulus versus density for the (**A**) p-PP systems and (**B**) graphitized p-PP systems, (**C**) bond density versus density for p-PP systems, and (**D**) elastic modulus as a function of hydrogen removal and density (the size of the points is proportional to the modulus) for the p-PP pathway 1 system; experimental data is for commercially available Solvay Thornel CF (*40*).

$$\text{change in } sp^3 \text{ fraction} = \frac{\text{final } sp^3 \text{ fraction} - \text{initial } sp^3 \text{ fraction}}{\text{initial } sp^3 \text{ fraction}} \quad (2)$$

where the final (initial) $sp^{2(3)}$ fraction is the final (initial) number of $sp^{2(3)}$ carbon atoms divided by the total number of carbon atoms. Further details are provided in the Supplementary Materials (sections S3 and S5). We note that the technique that we used to classify the bonds leads to an underestimation in the change in sp^3 fraction and an overestimation in the change in sp^2 fraction; the calculated fractions were a reasonable estimate of the true values. The changes in sp^2 and sp^3 fraction as a function of density for p-PP systems are plotted in Fig. 6A, and the corresponding correlation with elastic modulus is highlighted in Fig. 6B. Overall, we observed that increasing density corresponded to a higher fraction of sp^3 formation and lower fraction of sp^2 formation. This indicated that at higher densities, a higher fraction of sp^2 bonds was getting converted to sp^3 than vice versa. A similar phenomenon has been observed in diamond-like carbon systems (*41*). Moreover, because higher densities also led to higher elastic moduli, there exists a positive correlation between the change in sp^3 fraction and elastic modulus, as shown in Fig. 6B. A similar trend was also observed in CTP CFs, which is included in the Supplementary Materials (section S3).

Thus, like the reactions during graphitization that led to increased sp^2 bonds, the alternative high-density route corresponded to increased sp^3 bonds that can have an effect on the modulus. We observed around 54% sp^3 C fraction in an isotropic CTP CF sample that corresponds to a high elastic modulus of 146 GPa (section S11). Moreover, increased covalent cross-linking between different basal planes was reported to enhance the compressive properties of CFs (*1*, *42*). It has been shown that while low-modulus CFs fail in the buckling mode when subjected to compression, high-modulus CFs fail in the shear mode (*1*). These failure modes arise because of differences in intraplanar and interplanar connectivity. Introduction of sp^3 bonding is one method of improving interplanar connectivity, making it harder to shear (*1*). Overall, improved interplanar connectivity can result in improved mechanical properties of CFs (*1*, *42*). Figure 7 displays the angular distribution of sp^2 and sp^3 bonds in a sample of aligned PP CF. We observed that as the simulation proceeds, the bonds got more uniformly distributed with an overall increase in the number of bonds present at higher angles, which correspond to bonds perpendicular to the basal (*xy*) plane. This was especially prominent for sp^3 bonds, highlighting the increased interplanar connectivity. Similar angular distributions in other systems are included in the Supplementary Materials (section S7).

To gauge the impact of sp^3 bonding on compressive properties, we have additionally examined compressive modulus in this work. The tensile and compressive moduli for the small p-CTP and p-PP pathway 1 systems are depicted in Fig. 8. Similar results have been obtained in compressed glassy carbon systems; Hu *et al.* (*43*) observed sp^2 to sp^3 conversion upon compression to densities around 2.0 to 2.5 g/cm^3 along with compressive modulus as high as 330 GPa.

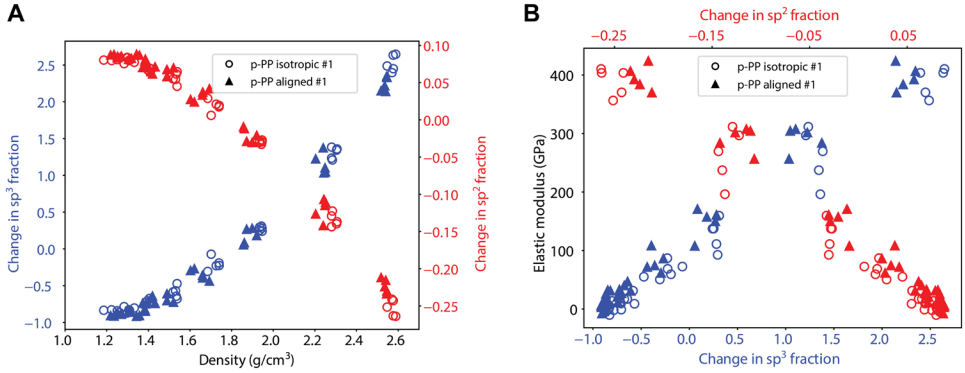

Fig. 6. Change in sp^2 and sp^3 fraction. (**A**) Change in sp^2 and sp^3 fraction as a function of density and (**B**) elastic modulus versus change in sp^2 and sp^3 fraction in p-PP pathway 1 system.

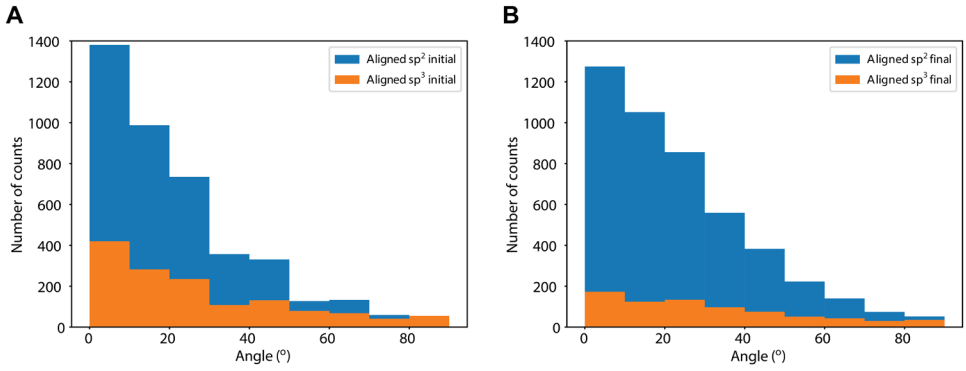

Fig. 7. Angular distribution of bonds. (**A**) Initial and (**B**) final angular distribution of sp^2 and sp^3 bonds in an aligned PP CF generated using pathway 1 with a final density of 1.92 g/cm^3; 0° corresponds to bonds parallel to the basal plane (*xy* plane). The final state shows that sp^3 bonds are more uniformly distributed across all orientations.

In the CTP aligned system (Fig. 8A), the tensile modulus was notably higher than its compressive counterpart, while the difference was not as pronounced in the PP system (Fig. 8B). In addition, in the PP system, the difference between aligned and isotropic CFs was much smaller than that in the CTP system. This can be explained from the methyl (sp^3) groups facilitating more interplanar connectivity, even in aligned PP CFs, while the aligned CTP CFs may not have as many interplanar connections arising from aromatic condensation reactions alone. Thus, in applications that require similar tensile and compressive moduli, PP CFs at high density can potentially outperform the low-density CFs obtained from graphitization (blue solid line instead of red in Fig. 5B). Moreover, given the remarkable similarity in the elastic modulus of both aligned and isotropic PP CFs, a potential for a modified CF fabrication process of isotropic CF that does not rely on consistent mesophase formation may be achieved with high-density isotropic PP.

DISCUSSION

The heterogeneous nature of the pitch precursors along with the large parametric space associated with the fabrication processes makes it challenging to optimize the procedure to generate CFs, resulting in a large variability in a range of mechanical properties, like the elastic modulus. In this work, we present a comprehensive solution by identifying the key chemical and processing parameters that determine and control the formation of pitch-based CFs through a general modeling framework that simulates and realistically reproduces the parameter phase space of CF synthesis from both CTP and PP precursors. The validation of the model in predicting modulus in relation to density through experiments is direct, with no fitting parameter and no assumptions in upscaling, for both CTP and PP CFs. ReaxFF with initial hydrogen removal works as strategy to model CF formation, as validated by comparison with experimental data. Moreover, by design, the experimental parameters such as the initial set of molecules for pitch, functional groups, molecular alignment, and density are directly used to define the parameter space within the modeling framework. We find that density, alignment, and functionality of the molecular constituents play an essential role in the CF mechanical properties, while the size and shape of the initial molecules play a less important role.

Furthermore, through these results, we propose novel synthesis strategies that can potentially lead to the fabrication of high-modulus CFs. First, we observed that increasing the density of the CFs results in higher modulus, suggesting an alternative path for high-modulus fibers other than graphitization. In addition, we find that isotropic CFs can be potentially fabricated with high tensile modulus by controlling the density of the CF during fabrication and therefore maximizing the interconnective bonding, either as sp^2 as in graphitic CF or as sp^3 as for ultrahigh-density isotropic fibers. Not coincidentally, the native isotropy of an sp^3-rich network in high-density isotropic CF results in compressive moduli that are comparable to their tensile counterparts, revealing exciting previously unused potential applications

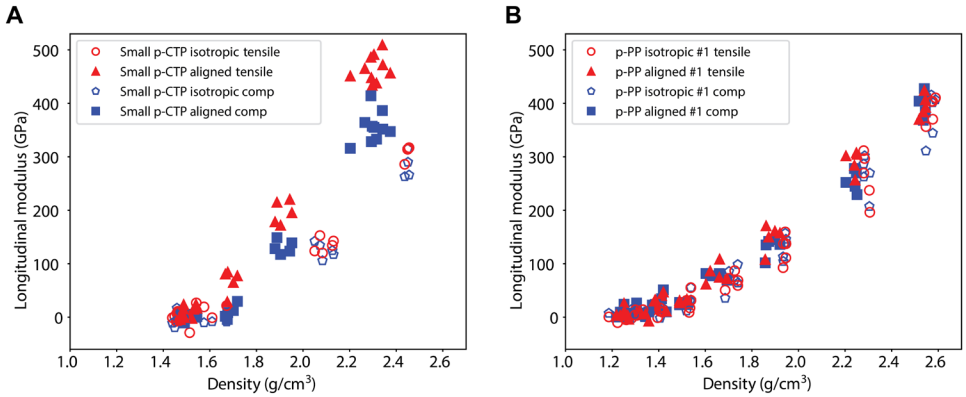

Fig. 8. Tensile and compressive moduli. Plotted as a function of density for (**A**) small p-CTP system and (**B**) p-PP pathway 1 system.

for CFs that rely on high compressive modulus, such as load-bearing building elements.

Each model in the computational framework is evaluated with unit cells on the order of a few nanometers, far from representing a complete micrometer-scale fiber. Yet, the modulus, as an atomic property, upscales from nanometer to larger scales, and excellent agreement is found with experimentally fabricated CFs (through this project or commercially available). However, other mechanical properties such as yield strength, fracture strength, and elongation cannot be equally estimated with the current framework without assumptions regarding the upscaling of the models from atomic to macroscale. For example, properties such as toughness, strength, and elongation that are affected by the microstructure (grain boundaries, surface fractures, voids, morphological inhomogeneities, etc.) require the assumption of the role of each at scales that are larger than those used in this work (*1*). This is hardly a limitation but rather an opportunity for future work: A robust predictive method for evaluating a large multitude of fibers and their synthesis conditions is the baseline condition to combine this framework with mesoscale and continuum modeling at the micrometer scale and beyond. As an extension of this model, other outputs like tensile and compressive transverse moduli, shear modulus, and Poisson's ratio have been obtained from this framework and can be used as an input for a mesoscale model that uses information of the fiber morphology to predict macroscale properties. In addition, a predictive capability of the modulus alone can be helpful for further modeling of specific fibers within this modeling framework that might be of interest, for example, to evaluate optimal stabilization conditions in a real fiber.

Ultimately, the most notable contribution from the proposed framework is in its ability to determine, hierarchically, the chemical and structural properties as well as processing parameters needed to achieve high-performance CFs, and how to compensate either at the precursor level or during synthesis to achieve manufacturing consistency. Furthermore, because the nanoscale models represent forms of carbon that are not unique to CFs, this framework can be modified and applied to other systems like films, coatings, and porous membranes (*39*, *44*, *45*), along with other carbonaceous materials like glassy carbons (*43*), and the insight of this work may provide additional insight on possible fabrication strategies to improve on their performance.

MATERIALS AND METHODS

In this work, we used MD simulations with ReaxFF using LAMMPS (Large-scale Atomic/Molecular Massively Parallel Simulator) (*46*–*48*) to generate CFs and subsequently calculate elastic modulus based on a stress-strain relationship. The ReaxFF developed by Chenoweth *et al.* (*27*) was used (see section S1 for further details). The visual molecular dynamics (VMD) was used for visualization (*49*). The molecular ensembles selected to represent specific representations of PP or CTP were packed in a $4 \times 4 \times 4$ nm^3 simulation box using PACKMOL (*50*).

Simulated stabilization and carbonization

A schematic of the procedure used is depicted in fig. S2. First, a fraction (default is 95%) of H atoms was removed at the start of the run. A Nosé-Hoover thermostat was used in constant-temperature simulations (*51*, *52*). All the systems were initially run at constant temperature of 3 K and at a constant volume. Next, the simulation box was compressed to smaller sizes in 2.5 ps while simultaneously heated from 3 to 300 K. The next step involved keeping the volume constant (the compressed state volume) and increasing the temperature from 3 to 300 K. This was followed by a volume relaxation, where the pressure and temperature were kept constant, which allowed the system to relax to its equilibrium volume. Compression and subsequent equilibration at 300 K allowed the activated molecules to come close enough to react, and by compressing the box to smaller sizes, we were able to generate CFs at higher densities. Generally, fibers are heated to around 200° to 500°C during stabilization and carbonization to allow for cross-linking by activating the sites. In this simulation, we activated the sites by removing a fraction of H initially, and thus, simulating the system to around 300 K sufficed to model stabilization and carbonization. Both removing H atoms initially and simulating at higher temperatures can be used to activate sites for cross-linking; as an example, in one specific case for a CTP model, we found that removing 95% H and heating to 300 K gave similar modulus as removing 50% H and heating to 1000 K. The procedure is listed in detail in the Supplementary Materials (section S1).

Simulated graphitization

To achieve very high elastic modulus (>300 GPa), graphitization is often used. This is achieved in this work by adding an additional step to the CFs generated at the end of the stabilization and carbonization.

CFs were first heated from 300 K to a high temperature (T_{high}, within a range of 3000 to 7000 K) in 5 ps at constant volume. This was followed by a run at constant volume and at constant temperature T_{high} for a graphitization time (t_{gra}) and subsequent cooling to 300 K in 5 ps. Here, we have varied t_{gra} in the range of 5 to 200 ps. Last, the system was equilibrated at 300 K for 2 ps at constant pressure, allowing it to relax to its equilibrated volume. By varying T_{high} and t_{gra}, we were able to generate graphitized CFs with a wide range of modulus and, eventually, optimize for T_{high} and t_{gra}. The procedure is listed in detail in the Supplementary Materials (section S4).

Experimental CF fabrication and testing

Pitch powder samples were spun into fibers using a barrel-and-plunger–type, single-filament extrusion system. A spinneret appointed with a single hole, 150 μm in diameter, and length (L)/diameter (D) ratio of 5 was used to produce the filament. Spinning temperatures were set to 40° to 50°C above the pitch softening point. Fibers were collected on a roll via a winder set to the maximum achievable speed in revolutions per minute where the fiber drawing remained stable for 5 min or more. Three-inch-long sectioned bundles of fibers were collected from the rolls, placed in a graphite crucible, and oxidized using optimized pathways for each sample established from previous studies (*53*–*57*). Oxidized fiber bundles were then transferred to a furnace and carbonized under streaming inert gas at a rate of 300°C/hour to a final temperature of 1200 to 1300°C. Tensile specimens from the best conversion pathways in each experimental pitch system were tested as single filaments in sets of 10 (*58*). Fiber density values used for validation were determined via the commonly used buoyancy method (*54*).

SUPPLEMENTARY MATERIALS

Supplementary material for this article is available at https://science.org/doi/10.1126/sciadv.abn1905

REFERENCES AND NOTES

1. S. Chand, Review Carbon fibers for composites. *J. Mater. Sci.* **35**, 1303–1313 (2000).
2. M. MInus, S. Kumar, The processing, properties, and structure of carbon fibers. *JOM.* **57**, 52–58 (2005).
3. T. Kraus, M. Kühnel, e Global CFRP Market. *Compos. Mark. Rep.* (2015).
4. B. A. Newcomb, Processing, structure, and properties of carbon fibers. *Compos. Part A Appl. Sci. Manuf.* **91**, 262–282 (2016).
5. S. Das, J. Warren, D. West, O. R. N. Laboratory, Global carbon fiber composites supply chain competitiveness analysis. *Tech. Rep.* , 116 (2016).
6. MetalMiner Prices, https://agmetalminer.com/metal-prices.
7. www.worldautosteel.org/projects/ulsab/process-cost-modeling.
8. D. Choi, H.-S. Kil, S. Lee, Fabrication of low-cost carbon fibers using economical precursors and advanced processing technologies. *Carbon N. Y.* **142**, 610–649 (2019).
9. CRU, www.itaorg.com/conference-pdfs/Global%20Coal%20Tar%20Pitch%20Market%20Outlook%20in%202021.pdf.
10. Petroleum Pitch Prices, www.intratec.us/chemical-markets/petroleum-pitch-price.
11. GEP, www.gep.com/blog/strategy/the-2019-global-outlook-for-acrylonitrile-will-the-supply-situation-improve.
12. H. G. Chae, B. A. Newcomb, P. V Gulgunje, Y. Liu, K. K. Gupta, M. G. Kamath, K. M. Lyons, S. Ghoshal, C. Pramanik, L. Giannuzzi, K. Şahin, I. Chasiotis, S. Kumar, High strength and high modulus carbon fibers. *Carbon N. Y.* **93**, 81–87 (2015).
13. D. D. Edie, The effect of processing on the structure and properties of carbon fibers. *Carbon N. Y.* **36**, 345–362 (1998).
14. F. T. Wallenberger, Ed., *Advanced inorganic fibers: Processes--structures--properties--applications* (Kluwer Academic, Boston, 2000), *Materials technology series*.
15. T. Matsumoto, Mesophase pitch and its carbon fibers. *Pure Appl. Chem.* **57**, 1553–1562 (1985).
16. X. Huang, Fabrication and properties of carbon fibers. *Materials (Basel).* **2**, 2369–2403 (2009).
17. J. Drbohlav, W. T. K. Stevenson, The oxidative stabilization and carbonization of a synthetic mesophase pitch, part II: The carbonization process. *Carbon N. Y.* **33**, 713–731 (1995).
18. S. Das, Opportunities and challenges for a domestc high-value coal products industry (2019).
19. M. Kowalik, C. Ashraf, B. Damirchi, D. Akbarian, S. Rajabpour, A. C. T. van Duin, Atomistic scale analysis of the carbonization process for c/h/o/n-based polymers with the ReaxFF reactive force field. *J. Phys. Chem. B* **123**, 5357–5367 (2019).
20. Q. Mao, S. Rajabpour, M. Kowalik, A. C. T. van Duin, Predicting cost-effective carbon fiber precursors: Unraveling the functionalities of oxygen and nitrogen-containing groups during carbonization from ReaxFF simulations. *Carbon N. Y.* **159**, 25–36 (2020).
21. B. Saha, G. C. Schatz, Carbonization in polyacrylonitrile (PAN) based carbon fibers studied by ReaxFF molecular Dynamics Simulations. *J. Phys. Chem. B* **116**, 4684–4692 (2012).
22. K. Joshi, M. I. Arefev, L. V Zhigilei, Generation and characterization of carbon fiber microstructures by atomistic simulations. *Carbon N. Y.* **152**, 396–408 (2019).
23. S. Desai, C. Li, T. Shen, A. Strachan, Molecular modeling of the microstructure evolution during carbon fiber processing. *J. Chem. Phys.* **147**, 224705 (2017).
24. L. Shi, M. Sessim, M. R. Tonks, S. R. Phillpot, Generation and characterization of an improved carbon fiber model by molecular dynamics. *Carbon N. Y.* **173**, 232–244 (2021).
25. T. Senda, Y. Yamada, M. Morimoto, N. Nono, T. Sogabe, S. Kubo, S. Sato, Analyses of oxidation process for isotropic pitch-based carbon fibers using model compounds. *Carbon N. Y.* **142**, 311–326 (2019).
26. C. Jian, J. J. Adams, J. C. Grossman, N. Ferralis, Carbon fiber synthesis from pitch: Insights from ReaxFF based molecular dynamics simulations. *Carbon N. Y.* **176**, 569–579 (2021).
27. K. Chenoweth, A. C. T. van Duin, W. A. Goddard, ReaxFF reactive force field for molecular dynamics simulations of hydrocarbon oxidation. *J. Phys. Chem. A* **112**, 1040–1053 (2008).
28. S. M. Zeng, T. Maeda, K. Tokumitsu, J. Mondori, I. Mochida, Preparation of isotropic pitch precursors for general purpose carbon fibers (GPCF) by air blowing—II. Air blowing of coal tar, hydrogenated coal tar, and petroleum pitches. *Carbon N. Y.* **31**, 413–419 (1993).
29. X. Fan, Y. Fei, L. Chen, W. Li, Distribution and structural analysis of polycyclic aromatic hydrocarbons abundant in coal tar pitch. *Energy Fuel* **31**, 4694–4704 (2017).
30. W. A. Burgess, J. J. Pittman, R. K. Marcus, M. C. Thies, Structural identification of the monomeric constituents of petroleum pitch. *Energy Fuel* **24**, 4301–4311 (2010).
31. D. F. Esguerra, W. P. Hoffman, M. C. Thies, Liquid crystallinity in trimer oligomers isolated from petroleum and pyrene pitches. *Carbon N. Y.* **79**, 265–273 (2014).
32. M. C. Thies, in *Polymer Precursor-Derived Carbon* (American Chemical Society, 2014; https://doi.org/10.1021/bk-2014-1173.ch005), vol. 1173 of *{ACS} {Symposium} {Series}*, pp. 85–136.
33. P. Chen, J. N. Metz, A. S. Mennito, S. Merchant, S. E. Smith, M. Siskin, S. P. Rucker, D. C. Dankworth, J. D. Kushnerick, N. Yao, Y. Zhang, Petroleum pitch: Exploring a 50-year structure puzzle with real-space molecular imaging. *Carbon N. Y.* **161**, 456–465 (2020).
34. C. Jian, S. Merchant, X. Zang, N. Ferralis, J. C. Grossman, Structural evolutions of small aromatic mixtures under extreme temperature conditions: Insights from ReaxFF molecular dynamics investigations. *Carbon N. Y.* **155**, 309–319 (2019).
35. J. Drbohlav, W. T. K. Stevenson, The oxidative stabilization and carbonization of a synthetic mesophase pitch, part I: The oxidative stabilization process. *Carbon N. Y.* **33**, 693–711 (1995).
36. A. Takaku, M. Shioya, X-ray measurements and the structure of polyacrylonitrile- and pitch-based carbon fibres. *J. Mater. Sci.* **25**, 4873–4879 (1990).
37. S. Schulze, P. A. Nikrityuk, B. Meyer, Porosity distribution in monodisperse and polydisperse fixed beds and its impact on the fluid flow. *Part. Sci. Technol.* **33**, 23–33 (2015).
38. Z. Yue, C. Liu, A. Vakili, Solvated mesophase pitch-based carbon fibers: Thermal-oxidative stabilization of the spun fiber. *J. Mater. Sci.* **52**, 8176–8187 (2017).
39. X. Zang, C. Jian, S. Ingersoll, H. Li, J. J. Adams, Z. Lu, N. Ferralis, J. C. Grossman, Laser-engineered heavy hydrocarbons: Old materials with new opportunities. *Sci. Adv.* **6**, eaaz5231 (2020).
40. www.matweb.com, Solvay Thornel.
41. J. Robertson, Mechanism of sp3 bond formation in the growth of diamond-like carbon. *Diamond Relat. Mater.* **14**, 942–948 (2005).
42. M. G. Northolt, L. H. Veldhuizen, H. Jansen, Tensile deformation of carbon fibers and the relationship with the modulus for shear between the basal planes. *Carbon N. Y.* **29**, 1267–1279 (1991).
43. M. Hu, J. He, Z. Zhao, T. A. Strobel, W. Hu, D. Yu, H. Sun, L. Liu, Z. Li, M. Ma, Y. Kono, J. Shu, H. Mao, Y. Fei, G. Shen, Y. Wang, S. J. Juhl, J. Y. Huang, Z. Liu, B. Xu, Y. Tian, Compressed glassy carbon: An ultrastrong and elastic interpenetrating graphene network. *Sci. Adv.* **3**, e1603213 (2017).
44. A. P. Straub, D. S. Bergsman, B. A. Getachew, L. M. Leahy, J. J. Patil, N. Ferralis, J. C. Grossman, Highly conductive and permeable nanocomposite ultrafiltration membranes using laser-reduced graphene oxide. *Nano Lett.* **21**, 2429–2435 (2021).

45. J. J. Patil, A. Jana, B. A. Getachew, D. S. Bergsman, Z. Gariepy, B. D. Smith, Z. Lu, J. C. Grossman, Conductive carbonaceous membranes: Recent progress and future opportunities. *J. Mater. Chem. A* **9**, 3270–3289 (2021).
46. http://lammps.sandia.gov, Sandia National laboratories.
47. S. Plimpton, Fast parallel algorithms for short-range molecular dynamics. *J. Comput. Phys.* **117**, 1–19 (1995).
48. S. A. P. A. Y. G. H. M. Aktulga, J. C. Fogarty, Parallel reactive molecular dynamics: Numerical methods and algorithmic techniques. *Parallel Comput.* **38**, 245–259 (2012).
49. W. Humphrey, A. Dalke, K. Schulten, VMD: Visual molecular dynamics. *J. Mol. Graph.* **14**, 33–38 (1996).
50. L. Martínez, R. Andrade, E. G. Birgin, J. M. Martínez, PACKMOL: A package for building initial configurations for molecular dynamics simulations. *J. Comput. Chem.* **30**, 2157–2164 (2009).
51. S. Nosé, A unified formulation of the constant temperature molecular dynamics methods. *J. Chem. Phys.* **81**, 511–519 (1984).
52. W. G. Hoover, Canonical dynamics: Equilibrium phase-space distributions. *Phys. Rev. A* **31**, 1695–1697 (1985).
53. S. H. Lee, S. M. Lee, U. Im, S.-D. Kim, S.-H. Yoon, B. Lee, D.-H. Peck, Y.-G. Shul, D.-H. Jung, Preparation and characterization of high-spinnability isotropic pitch from 1-methylnaphthalene-extracted low-rank coal by co-carbonization with petroleum residue. *Carbon N. Y.* **155**, 186–194 (2019).
54. S. Y. Jang, S. Ko, Y. P. Jeon, J. Choi, N. Kang, H. C. Kim, H.-I. Joh, S. Lee, Evaluating the stabilization of isotropic pitch fibers for optimal tensile properties of carbon fibers. *J. Ind. Eng. Chem.* **45**, 316–322 (2017).
55. X. Qin, Y. Lu, H. Xiao, Y. Wen, T. Yu, A comparison of the effect of graphitization on microstructures and properties of polyacrylonitrile and mesophase pitch-based carbon fibers. *Carbon N. Y.* **50**, 4459–4469 (2012).
56. J. L. Braun, K. M. Holtman, J. F. Kadla, Lignin-based carbon fibers: Oxidative thermostabilization of kraft lignin. *Carbon N. Y.* **43**, 385–394 (2005).
57. H. Shimanoe, T. Mashio, K. Nakabayashi, T. Inoue, M. Hamaguchi, J. Miyawaki, I. Mochida, S.-H. Yoon, Manufacturing spinnable mesophase pitch using direct coal extracted fraction and its derived mesophase pitch based carbon fiber. *Carbon N. Y.* **158**, 922–929 (2020).
58. K. M. Lyons, B. A. Newcomb, K. J. McDonald, H. G. Chae, S. Kumar, Development of single filament testing procedure for polyacrylonitrile precursor and polyacrylonitrile-based carbon fibers. *J. Compos. Mater.* **49**, 2231–2240 (2015).
59. C. Ashraf, A. C. T. van Duin, Extension of the ReaxFF combustion force field toward syngas combustion and initial oxidation kinetics. *J. Phys. Chem. A* **121**, 1051–1068 (2017).
60. A. Beste, ReaxFF study of the oxidation of lignin model compounds for the most common linkages in softwood in view of carbon fiber production. *J. Phys. Chem. A* **118**, 803–814 (2014).
61. D. Jiang, A. C. T. van Duin, W. A. Goddard, S. Dai, Simulating the initial stage of phenolic resin carbonization via the ReaxFF reactive force field. *J. Phys. Chem. A* **113**, 6891–6894 (2009).
62. S. Lu, C. Blanco, B. Rand, Large diameter carbon fibres from mesophase pitch. *Carbon N. Y.* **40**, 2109–2116 (2002).
63. P. Mérel, M. Tabbal, M. Chaker, S. Moisa, J. Margot, Direct evaluation of the sp3 content in diamond-like-carbon films by XPS. *Appl. Surf. Sci.* **136**, 105–110 (1998).

Acknowledgments

Funding: U.S. Department of Energy through the Consortium for Production of Affordable Carbon Fibers in the United States (grant DE-EE0008203). The research at Oak Ridge National Laboratory, managed by UT Battelle, LLC, for the U.S. Department of Energy (DOE) under contract DE-AC05-00OR22725, was sponsored by the Office of Energy Efficiency and Renewable Energy, Vehicle Technologies Office Program. Computational support was provided by the National Energy Research Scientific Computing Center (NERSC), a U.S. Department of Energy Office of Science User Facility located at Lawrence Berkeley National Laboratory, operated under contract no. DE-AC02-05CH11231. Computational support was also provided by Extreme Science and Engineering Discovery Environment (XSEDE), which is supported by National Science Foundation grant number ACI-1548562.

Author contributions: A.J., T.Z., and N.F. conceived the idea and approach presented in this work. A.J. and T.Z. performed the molecular simulations. T.Z. and Y.W. designed the initial computational procedure. A.J. performed the analysis. A.J., N.F., J.C.G., and Y.W. contributed to the interpretation of the computational results. J.J.A. provided insight on the molecular selection. Experiments were conducted by L.T.K. and J.J.A. N.F., L.T.K., and A.K.N. contributed to the interpretation of the experimental results. All authors contributed to the writing of the paper. **Competing interests:** The authors declare that they have no competing interests. **Data and materials availability:** All data needed to evaluate the conclusions in the paper are present in the paper and/or the Supplementary Materials.

Submitted 12 November 2021
Accepted 26 January 2022
Published 18 March 2022
10.1126/sciadv.abn1905